Homogeneous swarm of high-Reynolds-number bubbles rising within a thin gap. Part 1: Bubble dynamics

Emmanuella Bouche, Véronique Roig, Frédéric Risso, Anne-Marie Billet

Homogeneous swarm of high-Reynolds-number bubbles rising within a thin gap. Part 1: Bubble dynamics.

EMMANUELLA BOUCHE[1,3]
VÉRONIQUE ROIG [1,3]
FRÉDÉRIC RISSO [1,3]
ANNE-MARIE BILLET [2,3]

1 Institut de Mécanique des Fluides de Toulouse, Université de Toulouse (INPT, UPS) and CNRS. Allée C. Soula, Toulouse, 31400, France.
2 Laboratoire de Génie Chimique, Université de Toulouse (INPT,UPS) and CNRS. 4 allée E. Monso, BP74233, Toulouse cedex 4, 31432, France.
3 Fédération de recherche FERMaT, CNRS, Toulouse, France

The spatial distribution, the velocity statistics and the dispersion of the gas phase have been investigated experimentally in a homogeneous swarm of bubbles confined within a thin gap. In the considered flow regime, the bubbles rise on oscillatory paths while keeping a constant shape. They are followed by unstable wakes which are strongly attenuated due to wall friction. According to the direction that is considered, the physical mechanisms are totally different. In the vertical direction, the entrainment by the wakes controls the bubble agitation, causing the velocity variance and the dispersion coefficient to increase almost linearly with the gas volume fraction. In the horizontal direction, path oscillations are the major cause of bubble agitation, leading to a constant velocity variance. The horizontal dispersion, which is lower than that in the vertical direction, is again observed to increase almost linearly with the gas volume fraction. It is however not directly due to regular path oscillations, which are unable to generate a net deviation over a whole period, but results from bubble interactions which cause a loss of the bubble velocity time correlation.

Key Words: Include here the same key words that you chose from the list supplied on Manucript Central when you submitted the paper.

1. Introduction

A lot of chemical, biological or environmental applications involve bubble column technology for heat and mass exchangers or reactor devices. Bubbles are used to maximize interfacial area and enhance mixing. Their displacements induce liquid agitation that in turn influences the bubble distribution and velocity. A general understanding of this two-way coupling is fundamental. It is however particularly difficult to achieve since the

dynamics of bubbly flows depends on many parameters: characteristics of the flow in the absence of the bubbles, flow regimes of individual bubbles, presence of surfactants, confinement due to walls or inserts... Comprehensive investigations of well-defined elementary situations still appear to be necessary.

The present work focuses on a swarm of bubbles rising in a Hele-Shaw cell. The width of the gap is lower than the characteristic size of the bubbles, which are consequently strongly flattened. A thin liquid film is present between each side of a bubble and the corresponding wall. As in an unconfined bubble swarm, bubbles are thus free to move, even if their motions are restricted to the plane of the cell (Roig *et al.* 2011). This geometry is potentially of great interest for applications since, for a given size, the interfacial area of a bubble that is confined between two plates is enhanced compared to that of an unconfined bubble: it thus allows to obtain simultaneously a high-Reynolds-number flow with a good mixing efficiency and a large interfacial area favorable to transfers between phases (Roudet 2008). This configuration is also attractive for the general understanding of bubbly flows since it makes possible to study the agitation generated by large-Reynolds-number rising bubbles with unstable wakes while turbulence production is prevented by the strong confinement. Comparisons with unconfined situations are thus expected to be meaningful. Moreover, interface detection is considerably facilitated compared to classic three-dimensional cases because bubbles cannot hide each others: a complete and accurate description of bubble interfaces can therefore be obtained by means of a single camera facing the cell.

Some studies considered bubbly flows confined in a thin gap (Lin *et al.* 1996; Spicka *et al.* 2001) but they dealt with inhomogeneous bubble distribution and large flow recirculations. In this study, we aim at experimentally generating a swarm of high-Reynolds-number two-dimensional bubbles, with a homogeneous gas volume fraction over the whole cell and in the absence of significant mean liquid velocity. Our objective is to obtain a complete description of the gas dynamics in this particular configuration, which means to determine how bubbles *distribute*, *move* and *disperse*.

Let us summarize what is known concerning these three topics in three-dimensional swarms of bubbles at Reynolds numbers that are large enough for a significant wake to develop behind each bubble: $Re = Vd/\nu > 10$, where V is the mean bubble rising velocity, d is the bubble equivalent diameter and ν the kinematic viscosity of the liquid.

The spatial distribution of bubbles, even if we restrict ourselves to the case of a uniform gas volume fraction, is a complex issue. Hydrodynamic interactions between two spherical fixed bubbles have been studied theoretically and numerically for in-line bubbles (Yuan & Prosperetti 1994; Harper 1997), side-by-side bubbles (Legendre *et al.* 2003) and recently for a bubble pair with any orientation (Hallez & Legendre 2011). The results of these studies conclude that the side-by-side configuration is the only stable configuration. Computations, in the potential flow approximation, of a swarm of spherical bubbles that are free to move (Sangani & Didwania 1993; Smereka 1993; Yurkovetsky & Brady 1996) indeed show the formation of horizontal clusters, provided the bubble agitation is not too large. Direct numerical simulations with nearly spherical bubbles (Bunner & Trygvason 2002a; Esmaeeli & Trygvason 2005) also show the existence of horizontal clusters. Experiments at $Re = O(10)$ (Cartellier & Riviere 2001; Cartellier, Andreotti & Sechet 2009) indicate a deficit in the pair probability distribution function in the rear of the bubbles. Experiments with almost spherical bubbles at $Re = O(100)$ (Zenit *et al.* 2001; Figueroa-Espinoza & Zenit 2005) rising between two walls separated by a distance equal to a few bubble diameters show the existence of horizontal bubble clusters. However, it has been shown that the bubble distribution is significantly affected by the bubble deformation. Clusters are neither observed in the DNS of Esmaeeli & Trygvason (2005) for

Re=78 and We=3 nor in the experiments by Lance & Bataille (1991), Risso & Ellingsen (2002), Roig & Larue de Tournemine (2007) and Riboux *et al.* (2010) for air bubbles in water with diameters larger than 1.6 mm, which have strong wakes and experience path oscillations. Note that long-range preferential accumulation of bubbles in the vertical direction has been observed (Bunner & Trygvason 2003; Martinez Mercado *et al.* 2010) but is likely related to the generation of large-scale mean flow patterns that develop when the homogeneous case is not stable. It is also worth mentioning that strong clusters have been observed in the wall vicinity in the presence of surfactants (Takagi *et al.* 2008). For homogeneous bubble swarms at moderate to large Reynolds numbers, in the absence of mean flow and without strong surfactant effects, we can conclude that horizontal bubble clusters are observed provided bubble deformation remains small and strong unstable wakes do not develop. These clusters are most of the time rather weak and their lifetime has not been investigated in detail so far; their influence on the general flow dynamics is thus not clear. When bubble agitation induced by unstable bubble wakes develops, bubbles positions become almost independent from each others.

The bubble velocity is influenced by hydrodynamic interactions and evolves therefore with the gas volume fraction α. Most numerical (Bunner & Trygvason 2002a; Bunner & Trygvason 2003) and experimental (Zenit *et al.* 2001; Garnier *et al.* 2002; Roig & Larue de Tournemine 2007; Riboux *et al.* 2010) investigations of bubble swarms observed a decrease of the mean bubble velocity as α is increased. This phenomenon is generally attributed to the counter-flow generated within the interstitial space between the bubbles and their wakes, but the precise mechanism is however not understood yet. However, velocity fluctuations of a bubble is not only caused by the presence of the other bubbles. Due to wake instability, an isolated bubble rising at high Reynolds number is often observed to experience path oscillations (Ern *et al.* 2012). For air bubbles in water of d=2.5 mm, Risso & Ellingsen (2002) showed that the probability density function (PDF) of bubble velocities in a dilute bubble swarm (α=0.5%) is the same as that obtained by considering single rising bubbles with random phases and positions, which is strongly non Gaussian. At larger gas volume fractions, bubbles velocities are generally measured (Zenit *et al.* 2001; Garnier *et al.* 2002; Martinez Mercado *et al.* 2007; Riboux *et al.* 2010) by means of dual-probes that do not allow to make a clear distinction between the two components of the bubble velocity, the bubble rotation and the bubble deformation. However, it has been shown by Riboux *et al.* (2010) that wake instability of isolated bubbles can control and keep constant the energy of the bubble agitation up to a volume fraction of at least 12%. The precise evolutions of the corresponding PDF and of the relative weight of the vertical and horizontal components have not yet been fully characterized either from experiments or from numerical simulations. It is however clear that the bubble agitation strongly depends on the relative role played by self-induced oscillations and bubble-induced hydrodynamic disturbances, as well as by the interactions between these two phenomena.

The dispersion of the bubbles in a homogeneous swarm is an almost unexplored issue. As far as we know, it has never been addressed experimentally and has only been considered in two numerical studies (Bunner & Trygvason 2002b; Esmaeeli & Trygvason 2005), which found dispersion coefficients that increased with α and differed according to the considered directions. As for the bubble velocity, bubble dispersion may involve a contribution of self-induced oscillations and bubble-induced agitation.

In the present work, these three fundamental issues will be addressed from the experimental investigation of air bubbles rising within a thin gap filled with water. The case of the single two-dimensional rising bubble was investigated in a previous work (Roig *et al.* 2011), which described the various flow regimes that occurred when the bubble diam-

eter was increased from 2 to 30 mm. Here we have chosen to consider two-dimensional bubbles of about 4 mm ($Re \approx 500$) because their dynamics is close to that observed for three-dimensional bubbles of about 2 mm: sinusoidal path oscillations, almost constant elliptical shape, and similar liquid-velocity disturbances induced in the vicinity of a bubble (potential flow upstream and unstable wake behind). The evolution of the wake with the distance downstream of the two-dimensional bubble is however strongly attenuated. Although the wake of an unconfined isolated bubble of 2.5 mm extends up to more than 50 diameters (Ellingsen & Risso 2001), that of a confined bubble decays exponentially with a lengthscale approximately equal to 3-4 diameters. A great care has been taken to generate a swarm of such two-dimensional bubbles as homogeneous and monodisperse as possible by optimizing the bubble injection and preventing the coalescence.

The paper is organized as follows. Section 2 describes the experimental set-up, the operating conditions and the measurement methods. Section 3 is devoted to the spatial distribution of the bubbles, section 4 to the bubble velocity statistics and section 5 to the bubble dispersion.

2. Experimental set-up and instrumentation

The experimental set-up consists of a Hele-Shaw cell made of two vertical glass plates of size 800×400 mm^2, separated by a gap of width w= 1 mm (Fig. 1*a,b*). The cell is filled with distilled water to which 0.05 mol·L^{-1} of magnesium sulphate ($MgSO_4$) has been added. This small amount of electrolyte prevents coalescence from occurring without modifying significantly either the density, the viscosity or the surface tension of water (Tsao & Koch 1994).

The liquid is initially at rest and air bubbles are injected into the gap through a set of 16 capillary tubes of 0.6 mm inner diameter and 0.8 mm outer diameter. The capillary tubes are equally distributed all over the bottom of the cell to ensure a uniform gas volume fraction and avoid large-scale recirculations, so that the average liquid velocity, $\langle U \rangle$, is negligible everywhere in the cell. The tubes are connected to an air reservoir that is large enough to allow a stationary gas flow-rate. The gas volume fraction α can be varied from 1% to 14% by adjusting the flow-rate supplied to the reservoir.

The two-dimensional equivalent diameter of the bubbles, d, is defined as the diameter of the disk that has the same area, A, as the projection of the bubble onto the cell plane: $d = \sqrt{4A}/\pi$ (Fig. 1*b*). Figure 2 shows its probability density functions (PDF) for different values of α. The diameters are essentially distributed around a major peak, even if a tiny secondary peak, due to rare coalescence events, is observed for $\alpha \geqslant 7\%$. In the present configuration, coalescence can therefore be neglected. It is however worth mentioning that in preliminary tests carried out without $MgSO_4$, the coalescence was so intense that it was impossible to generate a stable bubble swarm. In contrast, coalescence was shown to be negligible in unconfined bubble swarm without $MgSO_4$ for a comparable range of parameters (Riboux *et al.* 2010). This difference suggests that the confinement changes the hydrodynamic interaction between bubbles. Here, the most probable diameter increases moderately from 3.9 to 4.6 mm as α increases from 1.4 to 13.6%. Moreover, almost all bubble diameters range between 3.5 and 5 mm for all volume fractions, which means that the relevant dimensionless groups lie in the following ranges:

- Archimedes number, $650 \leqslant Ar = \rho\sqrt{g\,d}\,d/\mu \leqslant 1100$,
- Bond number, $1.7 \leqslant Bo = \rho g d^2/\sigma \leqslant 3.5$,
- Reynolds number, $370 \leqslant Re = \rho V_0 d/\mu \leqslant 630$
- Weber number, $0.5 \leqslant We = \rho V_0^2/\sigma \leqslant 1$,
- gap to diameter ratio, $0.2 \leqslant w/d \leqslant 0.3$,

where g is gravity acceleration, ρ water density, μ water viscosity, σ surface tension and V_0 velocity of the bubble.

According to Roig *et al.* (2011), isolated bubbles with $600 \leqslant Ar \leqslant 1500$ belong to a single flow regime characterized by a constant elliptical shape with an aspect ratio close to 1.3 and path oscillations with bubble-centre velocity components given by

$$V_x(t) = V_0 + \tilde{V}_x \cos(2\omega t), \tag{2.1a}$$

$$V_y(t) = \tilde{V}_y \cos(\omega t + \phi), \tag{2.1b}$$

where $V_0 = 0.57\sqrt{gd}$, $\omega \approx 1.3V_0/d$, $\tilde{V}_x$ is close to $0.1V_0$ and $\tilde{V}_y$ to $0.45V_0$. These bubbles are followed by an unsteady wake with periodic vortex shedding. Both the wake and the vortices are damped by the wall friction, which causes them to decay exponentially with a timescale proportional to $T_\nu = w^2/\nu$. In particular, the velocity defect evolves with the distance x to the bubble as $V_0 \exp(-x/l_w)$ with $l_w = T_\nu V_0/7$.

For the present configuration, differences in the bubble size have thus not a significant influence on the dynamics and we will focus on the role of the gas volume fraction.

The shape, position and velocity of the bubbles are determined by processing of video images. The measurement window is a square of size 190×190 mm^2 located 350 mm above the tips of the capillary tubes and 100 mm under the top of the cell (Fig. 1*a*). The gas volume fraction and bubble velocity statistics have been checked to be uniform within this region. The cell is illuminated from behind by means of a panel of diodes which provides a homogeneous and constant light perpendicular to the cell plates. A high-speed camera (Photron RS3000) equipped with a 35-mm lens is placed on the other side of the cell, facing the lighting. It takes images of 1024×1024 pixels and 256 grey levels. The depth of field is larger than the gap and the pixel size is 185 ± 1 μm. Bubble contours are seen as fine dark shadows (Fig. 3) that are detected by applying a threshold to each recorded image – after subtraction of the background image obtained in the absence of bubbles. Images are then binarized and bubbles identified as blobs of pixels. A difficulty arises when bubbles come into contact and hence appear as merged blobs. Using what is *a priori* known about bubble size and shape, our algorithm allows nevertheless to identify individual bubbles in all cases. For each bubble i in a given image, the instantaneous bubble characteristics are determined. In particular, the area is obtained with an accuracy of ±17 pixels and the coordinates, x_i, y_i, of the centre of each bubble are measured with an accuracy of ±1 pixel.

Two different series of acquisition have been carried out. First, a frame rate of 1/4 fps has been used to collect at least 4,600 uncorrelated pairs of images for each gas volume fraction. This ensures the statistical convergence of the gas volume fraction, which is obtained from the bubble area, of the bubble spatial distribution, and of the bubble velocity. Second, samples of 25 s duration are recorded at 250 fps in order to continuously follow individual bubbles as they cross the measurement window. For that purpose, a tracking algorithm has been developed to recognize each bubble from image to image. Bubble trajectories are thus recorded and bubble velocity components, V_{x_i}, V_{y_i}, are obtained by differentiation with an accuracy of ±3 mm$\cdot$s^{-1}. Statistics of bubble velocities are finally computed from more than 20,000 events and dispersion characteristics from 1500 to 2500 bubble histories.

3. Spatial distribution of the bubbles

Even if the gas volume fraction is spatially uniform, bubble locations may not be statistically independent from each others. A way to address this point is to consider the

radial pair distribution function, $G(r)$, which measures the probability to find the centre of a bubble at a distance r from that of a given bubble (Fig. 1c). Here, it is estimated by counting the number of bubbles j located at a distance $r_{ij} = r \pm \Delta r$ from all bubbles i located within the circle of radius R having its center in the middle of the measurement window:

$$G(r) = \frac{\pi R^2}{N_b\,(N_b-1)}\,\frac{1}{2\,\pi\,r\,\Delta r}\sum_{i=1}^{N_b}\sum_{i=1,j\neq i}^{N_b} H(r_{ij}-r+\Delta r) - H(r_{ij}-r-\Delta r). \qquad (3.1)$$

$H(x)$ is the Heaviside function that is zero for $x < 0$ and unity for $x \geqslant 1$. $\Delta r = d/10$ is small enough to allow a good resolution. $R \approx 9d$ is less than one quarter of the measurement window side to avoid statistical biases related to finite size of the domain. N_b is the number of bubbles counted in the test section for all images, which is large enough (between 10^4 and 4×10^4 depending on α) to ensure statistical convergence for the chosen bin size, Δr. With this definition, $G(r)$ is unity when bubble locations are statistically independent, larger than one when there is an excess of bubbles and smaller when there is a deficit.

Figure 4 shows the evolution of $G(r/d)$ for various values of α from 1.4% to 13.6%. For rigid disks that cannot overlap, G should be equal to zero for $r/d < 1$. Here, since bubbles are ellipsoids that are free to move and rotate, bubble centers can get closer than d. Positive values of G are thus observed for $0.6 \leqslant r/d \leqslant 1$, especially at the largest values of α.

At the lowest gas volume fractions ($\alpha \leqslant 3.4\%$), the pair distribution function shows a significant deficit of bubble up to $4d$, which is approximately the distance between two injection tubes. The bubbles probably keep a memory of the injection conditions when there are not enough interactions before bubbles reach the measurement window. This effect vanishes as α is increased, only a weak deficit being still observed up to $2.5d$ at α=4.8%. For larger α, G is unity for any distance larger than $2d$.

At short distances ($d \leqslant r \leqslant 2d$), an accumulation of bubbles is observed when α becomes larger than 10%. At the largest investigated volume fraction (α=13.6%), G reaches a peak value of 1.16 at $1.5d$. Figure 5 compares the pair distribution functions computed for two different sample subsets with the vector connecting the bubble centers of each pair belonging to the subset limited by $\pm$ 45° either the horizontal direction (subset 1) or the vertical direction (subset 2). For α = 10%, there is no accumulation whatever the considered direction. For α=13.6%, the accumulation is essentially observed in the horizontal direction with a peak-value of 1.2 at $1.5d$, indicating a weak short-range preferential ordering of bubbles in this direction. These small clusters, which involve 2-3 bubbles, are less significant than those observed for three-dimensional bubbles by Figueroa-Espinoza & Zenit (2005) in the same ranges of Reynolds and Bond numbers. From visual inspection of video sequences, it can be seen that the present clusters are not persistent: they form and disappear as bubbles get closer and separate.

Provided injection conditions are forgotten (which is the case for $\alpha > 3.4\%$), it is observed that the position of a bubble is independent of the presence of other bubbles located at distances larger than 2d. Only a weak preferential ordering of bubbles is observed in the horizontal direction for smaller bubble distances at volume fractions larger than 10%. We can therefore conclude that bubble interactions do not alter significantly the spatial distribution of the bubbles.

4. Bubble velocity

We analyze now how hydrodynamic interactions may affect the bubble motions, starting with the average velocity before to consider fluctuations.

4.1. *Mean velocity*

Figure 6 shows the evolution with the gas volume fraction of the two components, $\langle V_x \rangle$ and $\langle V_y \rangle$, of the bubble average velocity. Since the mean liquid velocity is zero everywhere, these components also represent the mean velocity difference between the bubble and the liquid. They have been normalized by the average velocity of a single rising bubble, V_0, in order to focus on the role of the gas volume fraction. The measured horizontal component $\langle V_y \rangle$ is very small, confirming the satisfactory statistical convergence. The evolution of the vertical component $\langle V_x \rangle$ is more interesting: for α less than 4%, $\langle V_x \rangle / V_0$ remains almost unity; it then regularly increases by 12% as α increases from 4 to 10% and eventually reaches a constant value. Such an increase of the mean bubble velocity with the gas volume fraction was already observed by Spicka *et al.* (2001) in an unstable two-dimensional bubble column. It appears to be a particular feature of confined bubbly flows since a decrease of the bubble mean velocity is most often observed in unconfined situations, as discussed in the introduction and illustrated on the present figure by the measurements of Riboux *et al.* (2010). It is therefore clear that the hindrance effect that is often evoked to explain the evolution of the mean bubble velocity in three-dimensional situations is not relevant here.

This increase of the bubble velocity can however be understood by considering the average velocity of a bubble $\mathbf{V}_c(x, y)$ conditioned by the presence of another bubble located at the origin. Figure 7*a* shows the difference between this conditional average and the unconditional average in the vertical direction: $\Delta V_{c_x}(x, y) = (V_{c_x}(x, y) - \langle V_x \rangle)$. Here, $\Delta V_{c_x} / \langle V_x \rangle$ is represented for $\alpha = 2.3\%$, but its spatial structure is similar for all values of α. We observe that the velocity of bubbles rising in line is increased while that of side-by-side bubbles is decreased. The most important deviation in the vertical velocity is concentrated at the rear of the bubble. Figure 7*b*, shows the evolution of $\Delta V_{c_x}(x, 0) / \langle V_x \rangle$ along the symmetry axis behind the bubble for various gas volume fractions. Similarly to the wake of a single rising bubble, it decays exponentially as $\exp(-|x|/l_{rear})$ with a lengthscale close to the lengthscale l_w of the wake: $l_{rear} \approx 0.8 l_w$ for $\alpha \leqslant 4.8\%$ and $l_{rear} \approx 0.6 l_w$ for larger α. The change in the vertical velocity of a bubble is clearly related to the liquid disturbance generated by another bubble in its vicinity, which is mostly due to the bubble wake. Because its decay is controlled by the wall friction, this wake evolves weakly with the gas volume fraction and keeps the same structure as that of a single bubble.

We can also wonder if the short-range excess or deficit of bubbles observed in the radial pair distribution may contribute to the evolution of the bubble mean velocity with the gas volume fraction. To answer this question we have computed an unconditional averaged velocity $\langle \mathbf{V}_u \rangle$ from the measured conditional one, $\mathbf{V}_c(x, y)$, by assuming that bubble positions were independent to each others. The procedure is as follows. N_b bubble positions (x_i, y_i) are randomly chosen in a domain which has the same size as the measurement window, under only the constraint that bubbles must not overlap. N_b is fixed according to the prescribed value of α. The velocity of bubble i is given by

$$\mathbf{V}_i = V_0 \mathbf{e}_x + \frac{1}{N_b - 1} \sum_{j \neq 1} (\mathbf{V}_c(\mathbf{x}_i - \mathbf{x}_j) - V_0 \mathbf{e}_x), \tag{4.1}$$

where V_0 is the mean velocity of the single rising bubble ($\alpha = 0$), $\mathbf{V}_c$ is the conditional

bubble velocity at the corresponding value of α and $\mathbf{e}_x$ is the unit vertical vector. The unconditional average velocity for uniformly distributed bubbles is then obtained by summation of all individual bubble velocities,

$$\langle \mathbf{V}_u \rangle = \frac{1}{N_b} \sum_{i=1}^{N_b} \mathbf{V}_i. \tag{4.2}$$

The two components $\langle V_{ux} \rangle$ and $\langle V_{uy} \rangle$ are represented by dashed lines on figure 6. They perfectly match the measurements, proving that small departures to the ideal bubble distribution plays no role in the evolution of the bubble mean velocity.

Now it has been shown that the main mechanism is the entrainment by the wake, the evolution of the mean vertical bubble velocity with α can be interpreted. For α less than 4%, the average distance between two bubbles, $\delta \sim d\alpha^{-1/2}$, is larger than the wake length $l_w \approx 4d$; very few bubbles enter into the wake of another bubble and $\langle V_x \rangle$ remains close to V_0. For α between 4 and 10%, more and more bubbles are located into wakes and $\langle V_x \rangle$ is observed to increase. Due to their small extension, the wakes are rapidly filled up by bubbles and $\langle V_x \rangle$ attains a maximal value at larger values of α.

4.2. *Velocity fluctuations*

We consider now the time fluctuations v'_x and v'_y of the two components of the bubble velocity.

Figure 8 shows their standard deviations $\langle {v'_x}^2 \rangle^{1/2}$ and $\langle {v'_y}^2 \rangle^{1/2}$ against the gas volume fraction. The results at α=0 (grey squares and circles) have been measured for single rising bubbles, they hence correspond to the reference situation in the absence of any hydrodynamic interactions. These fluctuations are the signature of the bubble path oscillations described by Eq. (2.1), which are generated by vortex shedding and mainly occur in the horizontal direction. Measurements in the bubble swarm configuration have been obtained from α=1.4% up to 13.6%. The two components show totally different behaviors.

For any value of α, the horizontal component keeps a constant value equal to that of a single bubble: $\langle {v'_y}^2 \rangle^{1/2} \approx 0.45 V_0$. This suggests that the agitation of the bubbles in the horizontal direction remains caused by the vortex shedding, the intensity of which is not altered by the presence of the other bubbles. A similar trend has already been observed for three dimensional bubbles, as illustrated by the measurements of Riboux *et al.* (2010) which are reported in the present figure. It is important to mention that the measurements in the three dimensional swarm correspond neither to the horizontal nor the vertical velocity fluctuation but are a measure of the global bubble agitation that includes motion, rotation and deformation – in which the vertical velocity fluctuation probably takes a minor part.

On the other hand, the vertical standard deviation, $\langle {v'_x}^2 \rangle^{1/2}$, regularly increases from $0.1V_0$ at α=1.4% up to $0.3V_0$ at α=13.6%, although it remains always less than the horizontal one. Even if we ignore what occurs between α=0 and α=1.4%, it is intriguing that the extrapolation of the measurements done within the bubble swarm do not seem to join the value corresponding to isolated bubbles. Moreover, preliminary measurements of the liquid velocity show that the standard deviation of the vertical liquid velocity scales as $\alpha^{0.46}$. Such a scaling, represented by the dashed line on figure 8, also gives a reasonable fit of $\langle {v'_x}^2 \rangle^{1/2}$. This agreement between liquid and bubble fluctuations suggests that the intensity of the bubble agitation in the vertical direction is controlled by hydrodynamic interactions, provided the gas volume fraction is not too small.

Additional insights are obtained by considering probability density functions. Figure 9 shows the PDFs of the vertical and horizontal bubble velocity fluctuations normalized by their standard deviations, in both linear and semilog plots, for various gas volume fractions. Again, the two components show very different behaviors.

Let us consider first the horizontal direction (Fig. 9*b*&*d*). At the lowest gas volume fraction (α=1.4%), the PDF of v'_y takes the typical double-peak shape of the sine function. As α increases the maximum values slowly decrease and the gap between the peaks is progressively filled. It is only at the largest volume fraction (α=13.6%) that the PDF becomes almost Gaussian. Since the standard deviation, $\langle {v'_y}^2 \rangle^{1/2}$, remains constant, the process can be interpreted as follows. Side-by-side interactions, which only occur at very short distances, disturb the phase of the bubble oscillatory motions without changing their energy which remains controlled by the intensity of the vortex shedding. In the horizontal direction, the role of hydrodynamic interactions on the bubble fluctuations is thus restricted to make oscillations progressively loss their time coherence as the gas volume fraction is increased.

The PDFs of vertical fluctuations follow a radically different trend (Fig. 9*a*&*c*). A weak footprint of the double-peak shape is only discernible at α=1.4%. Then the PDF of v'_x adopts the typical behavior of liquid velocity fluctuations in bubbly flows: asymmetric shape almost invariant with α with large upward fluctuations more probable than large downward ones. This confirms that vertical bubble fluctuations are controlled by vertical liquid fluctuations.

5. Bubble dispersion

The two-dimensional bubble swarm is particularly well suited to investigate the Lagrangian bubble statistics since it allows to track the bubbles continuously along their path. In figure 10, different individual bubble trajectories have been superimposed by defining the origin as the position where they are detected for the first time within the measurement window. Subfigure (a) shows the paths of two single rising bubbles. We observe nice regular oscillations around the vertical direction, which means that path oscillations generated by vortex shedding are not able to disperse bubbles in the absence of interactions with other bubbles. Subfigure (b) and (c) show 1,000 bubble trajectories recorded for α=2.1% and α=13%, respectively. The horizontal bubble dispersion can be appreciated from the envelope of the different paths: it is clearly larger at the largest gas volume fraction.

In order to make a quantitative description, let us introduce the difference between the bubble-centre position at instant t and the average displacement of the bubbles during the same time interval: $(x'(t), y'(t)) = (x(t), y(t)) - (\langle x(t) \rangle, \langle y(t) \rangle)$, where the time origin is the instant when all these quantities vanish. Figure 11 shows the PDFs of $x'(t)$ and $y'(t)$ normalized by their respective standard deviations $\langle x'(t)^2 \rangle^{1/2}$ and $\langle y'(t)^2 \rangle^{1/2}$. Results for two different times (t = 0.2 s, t = 0.6 s) and various gas volume fractions between 3.2% and 13% are presented. In all cases, no significant departure from the Gaussian distribution is visible. The knowledge of the variances $\langle x'(t)^2 \rangle$ and $\langle y'(t)^2 \rangle$ is therefore sufficient to fully characterize these PDFs.

Other important quantities for the dispersion are the Lagrangian autocorrelation coefficients, $C_{xx}(\tau) = \langle v'_x(t) v'_x(t+\tau) \rangle / \langle {v'_x}^2 \rangle$ and $C_{yy}(\tau) = \langle v'_y(t) v'_y(t+\tau) \rangle / \langle {v'_y}^2 \rangle$. They are plotted in figure 12 for various gas volume fractions. In the horizontal direction, C_{yy} is a damped cosine function. Its period is independent of α and equals to that of the oscillation of an isolated bubble, $T_{osc} = 2\pi/\omega \approx 0.17$ s, whereas its damping rate is

an increasing function of α. This confirms the interpretation of horizontal bubble fluctuations proposed in the previous section: bubble oscillations remain driven by vortex shedding but lose progressively their time correlation due to hydrodynamic interactions as α increases. In the vertical direction, the behavior of the correlation is very different. In contrast with C_{yy}, C_{xx} is not symmetric about the time axis. The damped cosine function is still present, with a period which corresponds to that of the oscillation of an isolated bubble in the vertical direction (half that in the horizontal direction). However, it constitutes only a minor contribution to the correlation. The main contribution is now a positive decreasing function as expected for a particle in a turbulent flow. Moreover, the damping of the cosine contribution of C_{xx} is much larger than that of C_{yy}, so the oscillating part has almost completely vanished at α=13%.

The efficiency of the dispersion in both directions is measured by the dispersion coefficients,

$$D_x = \frac{1}{2}\frac{d\langle x'^2\rangle}{dt} = \langle v_x'^2\rangle\, T_x \quad \text{and} \quad D_y = \frac{1}{2}\frac{d\langle y'^2\rangle}{dt} = \langle v_y'^2\rangle\, T_y, \tag{5.1}$$

where the variance of the displacements $\langle x'^2\rangle$ and $\langle y'^2\rangle$ are considered at times that are large compared to the Lagrangian integral timescales, which are defined by $T_x = \int_0^\infty C_{xx}(\tau)\,\mathrm{d}\tau$ and $T_y = \int_0^\infty C_{yy}(\tau)\,\mathrm{d}\tau$. Figure 13 shows the evolution of $\langle x'^2\rangle$ and $\langle y'^2\rangle$ with t. As excepted from the trajectories (Fig. 10) and the autocorrelations (Fig. 12), the horizontal variance $\langle y'^2\rangle$ shows oscillations that decrease as α increases while oscillations are hardly visible in the evolution of the vertical variance $\langle x'^2\rangle$, even at the lowest gas volume fraction. These oscillations however play no role in the dispersion which is controlled by the global increases of the variances. Here, $\langle x'^2\rangle$ and $\langle y'^2\rangle$ have been normalized by $\langle v_x'^2\rangle$ and $\langle v_y'^2\rangle$ so that the slopes of the curves may directly correspond to the Lagrangian integral timescales. For each value of α, T_x and T_y can been determined either from the integral of the autocorrelation coefficients or from the derivative of the normalized displacement variances for t larger than 0.7 s after filtering residual oscillations out. We have checked that the two methods give the same results and will present here only values computed from the slopes. T_x and T_y are plotted against the gas volume fraction in the insets. If we exclude the lowest gas volume factions ($\alpha < 3\%$), the vertical timescale is observed to be constant, $T_x \approx 0.21$ s, whereas the horizontal one increases linearly as $0.33\,\alpha$ s. Figure 14 shows the evolution of the dispersion coefficients, D_x and D_y, with the gas volume fraction. Both evolve almost linearly with α even if the dispersion is much more efficient in the vertical direction. Considering they are the product of velocity variance by the Lagrangian timescale (Eq. 5.1), it however appears clearly that the physical mechanisms are very different in the two directions.

In the vertical direction, T_x is almost constant (Fig. 13) whereas $\langle v_x'^2\rangle$ evolves almost linearly with α. Assuming $T_x = 0.21$ s and $\langle v_x'^2\rangle = 7.4 \times 10^{-3}\,\alpha^{0.92}$ m^2·s^{-2} (which is the fit proposed in Fig. 8), we indeed get the reasonable fit of D_x drawn in figure 14. (At the largest volume fraction, the fit deviates from the measurements due to a small decrease of T_x.) The increase of D_x with α is thus mainly due to that of $\langle v_x'^2\rangle$. This behavior can be understood by considering what we have learnt about the bubble velocity. Conditional averaging of the bubble velocity shows that the major effect of bubble interactions is entrainment by the wakes. Moreover, the length, l_w, and the intensity of the wake only weakly depends on the gas volume fraction. This has two consequences. First, when the total number of bubbles is increased, the number of bubbles within the wakes is increased in the same proportion, which explains why $\langle v_x'^2\rangle$ increases almost linearly with α. Second, the Lagrangian timescale T_x corresponds to the time spent by a bubble within the wake of another bubble: it scales as l_w/V_0 (≈ 0.15 s) and is therefore almost independent of α.

In the horizontal direction, the roles are reversed, the variance is constant and the integral timescale is proportional to the gas volume fraction. The fit of D_y in figure 14 is obtained by the product of $\langle v_y'^2 \rangle \approx 2.6 \times 10^{-3}$ m^2·s^{-2} (Fig. 8) and $T_y = 0.33\,\alpha$ s (Fig. 13). As discussed earlier, the agitation of the bubbles in the horizontal direction is driven by wake-induced oscillations. Its energy, measured by $\langle v_y'^2 \rangle$, is therefore independent of α. On the other hand, horizontal velocity oscillations centered around zero are not able to disperse bubbles. However, each time a bubble gets very close to another bubble, the regular oscillations are perturbed and the bubble deviates from this vertical average path. The integral timescale T_y is thus controlled by the rate at which a bubble encounters other bubbles along its rising path, which is an increasing function of the gas volume fraction. The horizontal bubble dispersion thus results from a loss of time coherence of bubble oscillations due to hydrodynamic interactions.

6. Conclusion

The dynamics of the gas phase has been investigated in a homogeneous swarm of bubbles rising within a Hele-Shaw cell for gas volume fractions between 1 % and 14 %. In the considered flow regime, inertia plays a major role (Re ≈500). Each bubble is followed by unstable wake where a regular vortex shedding occurs, and rises along an oscillatory path while keeping an almost constant elliptical shape. However, in contrast to what is observed in unconfined situations, the wake is strongly attenuated by the wall friction and has almost vanished at only 4 diameters behind a bubble.

The spatial distribution of the bubbles remains very close to the ideal situation where bubble locations are independent to each others. Only small departures to this ideal have been detected. There are however limited to bubble separations less than two diameters and have negligible influence on statistics of the bubble dynamics. Two phenomena control the statistics of the bubble motions: the wake-induced oscillations and the strong velocity disturbances localized at the bubble rears. Depending on the direction that is considered, the relative importance of these two phenomena is changed and the physical mechanisms are totally different.

In the vertical direction, the principal mechanism is the entrainment by the wakes. First, it induces an increase of the mean bubble rise velocity, which remains however slight probably because it is partly counterbalanced by the classic hindrance effect observed in unconfined situations. Second, it causes an almost linear increase of the variance of the vertical bubble velocity as the gas volume fraction is increased. This linearity comes from the fact that the bubble wake remains almost unchanged as α increases whereas the probability that a bubble is located within the wake of another bubble is proportional to α. Finally, wake entrainment generates a vertical dispersion of the bubble characterized by a dispersion coefficient with is almost proportional to α. Indeed, since no stable clusters are formed, the time spent by a bubble in the wake of another bubble does not depend on the gas volume fraction. The evolution of the vertical dispersion coefficient of the bubbles with the gas volume fraction is thus driven by that of the bubble velocity variance.

In the horizontal direction, the bubble agitation is essentially caused by the wake-induced oscillations, the intensity of which is independent of the gas volume fraction. As a consequence, the variance of the bubble velocity is independent of α. Sinusoidal oscillations are unable to cause dispersion. However, random interactions between bubbles, by causing the decay of the sinusoidal time correlation of the bubble velocity, generate a horizontal bubble dispersion, which increases as the rate at which a bubble is perturbed by an other bubble. The horizontal diffusion coefficient is also found to increases linearly with α but remains smaller than that in the vertical direction.

Thanks to the advantages of a two-dimensional configuration for optical measurements, we have been able to draw a quite comprehensive picture of the mechanisms controlling the bubble dynamics. Unfortunately, such a detailed description is not available in unconfined flow, especially concerning bubble dispersion. It is thus not possible to conclude definitively concerning the differences between three-dimensional and two-dimensional configurations. It seems however very likely that the mechanisms related to wake entrainment and bubble path oscillations are major mechanisms in three-dimension too. Their relative importance according to each direction is however probably different. In particular, the predominance of the wake entrainment in the vertical direction, which causes the mean bubble velocity to increase with the gas volume fraction, is probably specific to two-dimensional flows.

Further insights into this matter will be obtained from the investigation of the dynamics of the liquid phase.

This work was supported by CNRS and the lab federation FERMaT.

REFERENCES

Bunner B. & Tryggvason G. 2002 Dynamics of homogeneous bubbly flows. Part 1. Rise velocity and microstructure of the bubbles *J. Fluid Mech.* **466**, 17–52.

Bunner B. & Tryggvason G. 2002 Dynamics of homogeneous bubbly flows. Part 2. Velocity fluctuations *J. Fluid Mech.* **466**, 53–84.

Bunner B. & Tryggvason G. 2003 Effect of bubble deformation on the properties of bubbly flows *J. Fluid Mech.* **495**, 77–118.

Cartellier, A., Riviere, N. 2001 Bubble-induced agitation and microstructure in uniform bubbly flows at small to moderate particule Reynolds numbers. *Physics of Fluids* **13, 8**, 2165–2181.

Cartellier, A., Andreotti & M., Sechet, P. 2009 Induced agitation in homogeneous bubbly flows at moderate particle Reynolds number. *Physical Rev. E* **80**, 065301(R).

Ellingsen K. & Risso F. 2001 On the rise of an ellipsoidal bubble in water: oscillatory paths and liquid-induced velocity *J. Fluid Mech.* **440**, 235–268.

Ern P., Risso F., Fabre D., Magnaudet J. 2012 Wake-Induced Oscillatory Paths of Freely Rising or Falling Bodies. *Annual Review of Fluid Mechanics* **44, 1**.

Esmaeeli A. & Tryggvason G. 2005 A direct numerical simulation study of the buoyant rise of bubbles at O(100) Reynolds number. *Phys. Fluids* **17**, DOI 093303.

Figueroa-Espinoza B. & Zenit, R. 2005 Clustering in high Re monodispersed bubbly flows *Phys. Fluids* **17**, DOI: 10.1063/1.2055487.

Garnier C., Lance M., Marié J.L. 2010 Measurement of local flow characteristics in buoyancy-driven bubbly flow at high void fraction. *Exp. Therm. Fluid Sc.* **26**, 811–815.

Hallez, Y. & Legendre, D. 2011 Interaction between two spherical bubbles rising in a viscous liquid *J. Fluid Mech.* **673**, 406–431.

Harper, J. F. 1997 Bubbles rising in line: why is the first approximation so bad? *J. Fluid Mech.* **351**, 289–300.

Lance, M. & Bataille J. 1991 Turbulence in the liquid phase of a uniform bubbly air water flow. *J. Fluid Mech.* **222**, 95-118

Legendre D., Magnaudet J., Mougin G. 2003 Hydrodynamic interactions between two spherical bubbles rising side by side in a viscous liquid *J. Fluid Mech.* **497**, 133–166.

Lin T.-J., Reese J., Hong T., Fan L.-S. 1996 Quantitative analysis and computation of two-dimensional bubble columns. *AIChE Journal* **42**, 2, 301–318.

Martinez Mercado J., Palacios-Morales C. A., Zenit R. 2007 Measurements of pseudo-turbulence intensity in monodispersed bubbly liquids for 10¡Re¡500. *Phys. Fluids* **19**, DOI: 10.1063/1.2772256.

Martinez Mercado J., Chehata Gomez D., van Gils D., Sun C., Lohse D. 2010 On bubble clustering and energy spectra in pseudo-turbulence. *J. Fluid Mech.* **650**, 287–306.

Riboux G., Risso F., Legendre D. 2010 Experimental characterization of the agitation generated by bubbles rising at high Reynolds number. *J. Fluid Mech.* **643**, 509–559.

Risso, F. & Ellingsen, K. 2002 Velocity fluctuations in a homogeneous dilute dispersion of high-Reynolds-number rising bubbles. *J. Fluid Mech.* **453**, 395–410.

Risso F., Roig V., Amoura Z., Riboux G., Billet A.M. 2008 Wake attenuation in large Reynolds number dispersed two-phase flows. *Phil. Trans. R. Soc. A* **366**, 2177-2190

Roig V., Larue de Tournemine A. 2007 Measurement of interstitial velocity of homogeneous bubble flows at low to moderate void fraction. *J. Fluid Mech.* **572**, 87-110

Roig V., Roudet M., Risso F., Billet A. M. 2011 Dynamics of a high-Reynolds-number bubble rising within a thin gap. *J. Fluid Mech.* , submitted

Roudet M., Billet A. M., Risso F., Roig V. 2011 PIV with volume lighting in a narrow cell: An efficient method to measure large velocity fields of rapidly varying flows. *Experimental Thermal and Fluid Science* **vol. 35, issue 6**, 1030–1037.

Roudet M. 2008 Hydrodynamique et transfert de masse autour dúne bulle confinée entre deux plaques. *PhD of the University of Toulouse, France.*

Sangani, A. S., & Didwania, A. K. 1993 Dynamic simulations of flows of bubbly liquids at large Reynolds numbers. *J. Fluid Mech.* **250**, 307–337.

Smereka, P. 1993 On the motion of bubbles in a periodic box. *J. Fluid Mech.* **254**, 79–112.

Spicka P., Dias M. M., Lopes J. C. B. 2001 Gas-liquid flow in a 2D column: Comparison between experimental data and CFD modelling. *Chem. Eng. Science* **56**, 6367–6383.

Takagi, S., Ogasawara, T. & Matsumoto, Y. 2008 The effects of surfactant on the multiscale structure of bubbly flows. *Phil. Trans. R. Soc. A* **366**, 2117–2129.

Tsao H-K. & Koch, D. L. 1994 Collisions of slightly deformable, high Reynolds number bubbles with short-range repulsive forces. *Phys. Fluids* **6**, 2591–2625.

van Winjgaarden L. 2005 Bubble velocities induced by trailing vortices behind neighbours. *J. Fluid Mech.* **541**, 203–229.

Yuan, H. & Prosperetti, A. 1994 On the in-line motion of two spherical bubbles in a viscous fluid. *J. Fluid Mech.* **278**, 325–349.

Yurkovetsky, Y. & Brady, J. F. 1996 Statistical mechanics of bubbly liquids. *Phys. Fluids* **8**, 881–895.

Zenit R. & Koch, D. L., Sangani A. S. 2001 Measurements of the average properties of a suspension of bubbles rising in a vertical channel. *J. Fluid Mech.* **429**, 307–342.

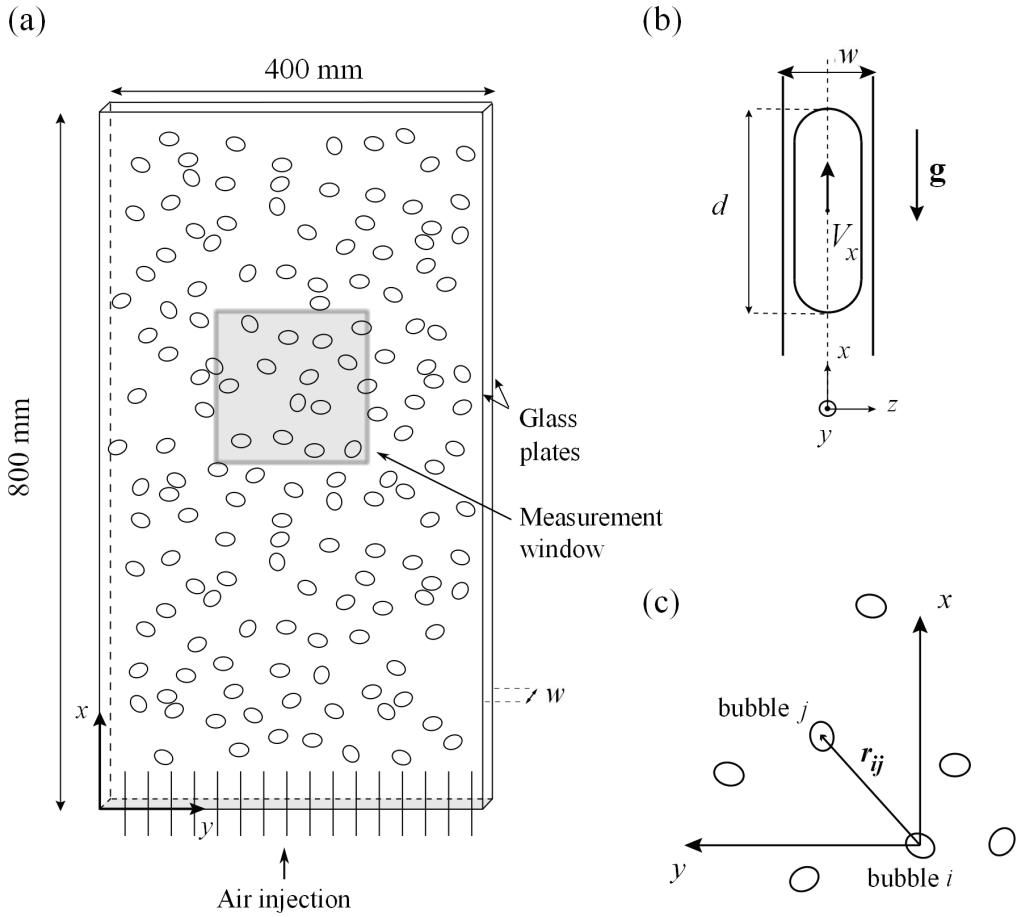

FIGURE 1. (a) Schematic view of the cell (bubbles are not to scale). (b) Side view of a bubble with a vertical velocity V_x, rising within the gap. (c) Definition of the vector $\mathbf{r}_{ij}$ joining the centroids of bubbles i and j.

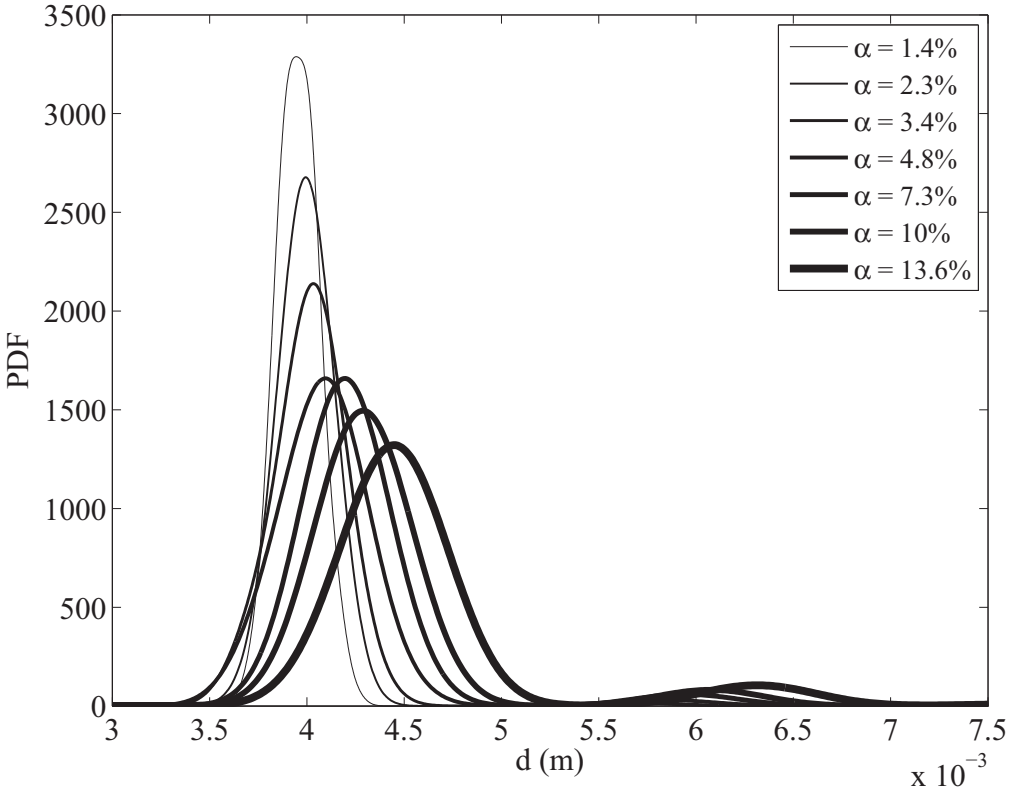

FIGURE 2. Probability density functions of the equivalent diameter for different gas volume fractions ranging from 1.4% to 13.6%.

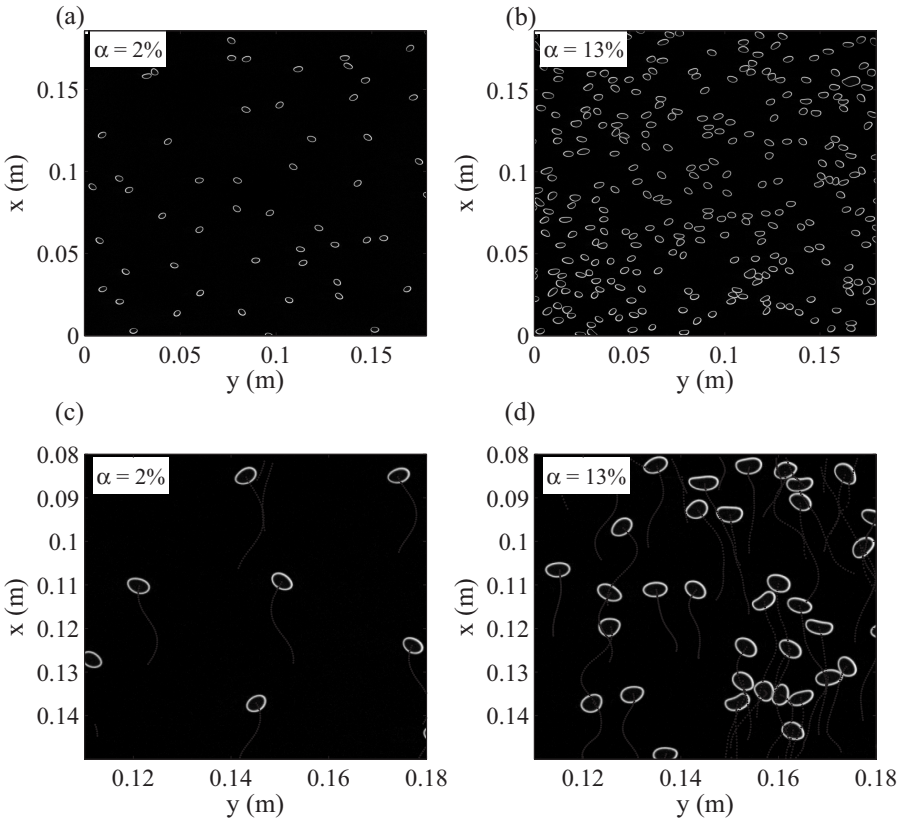

FIGURE 3. Images of bubble swarms after subtraction of the background image. (a), α=2%; (b), α =13%; (c) and (d) are zooms of (a) and (b) with bubble trajectories recorded during 0.16 s.

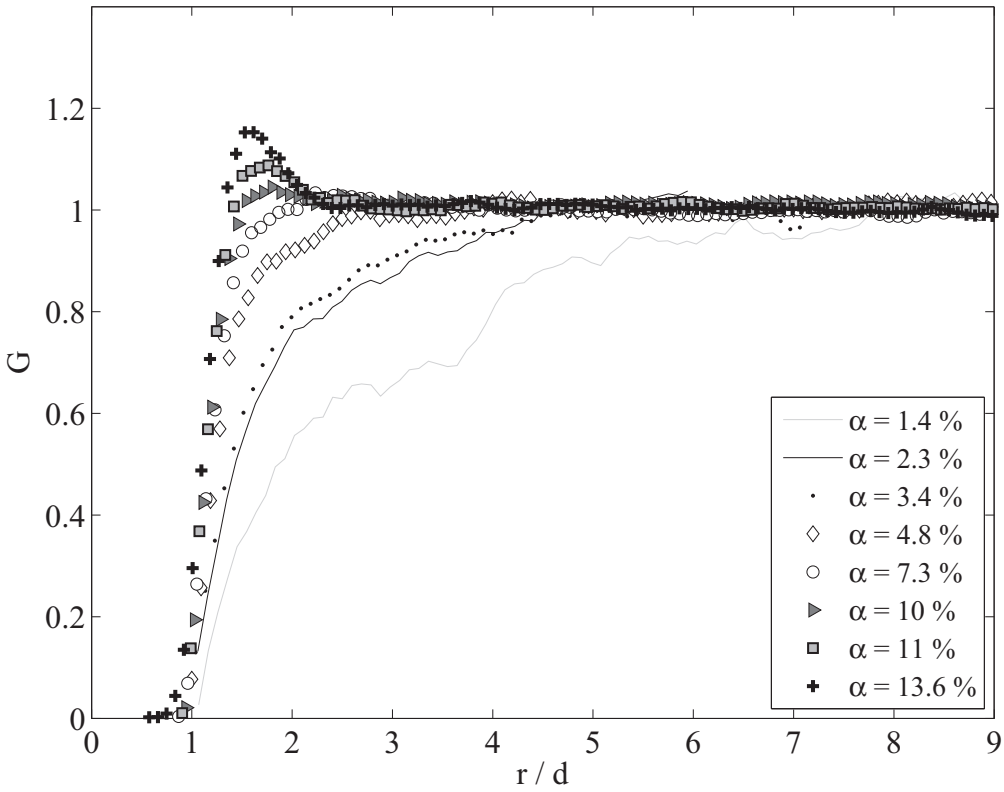

FIGURE 4. Radial pair distribution function G against r/d for various gas volume fractions.

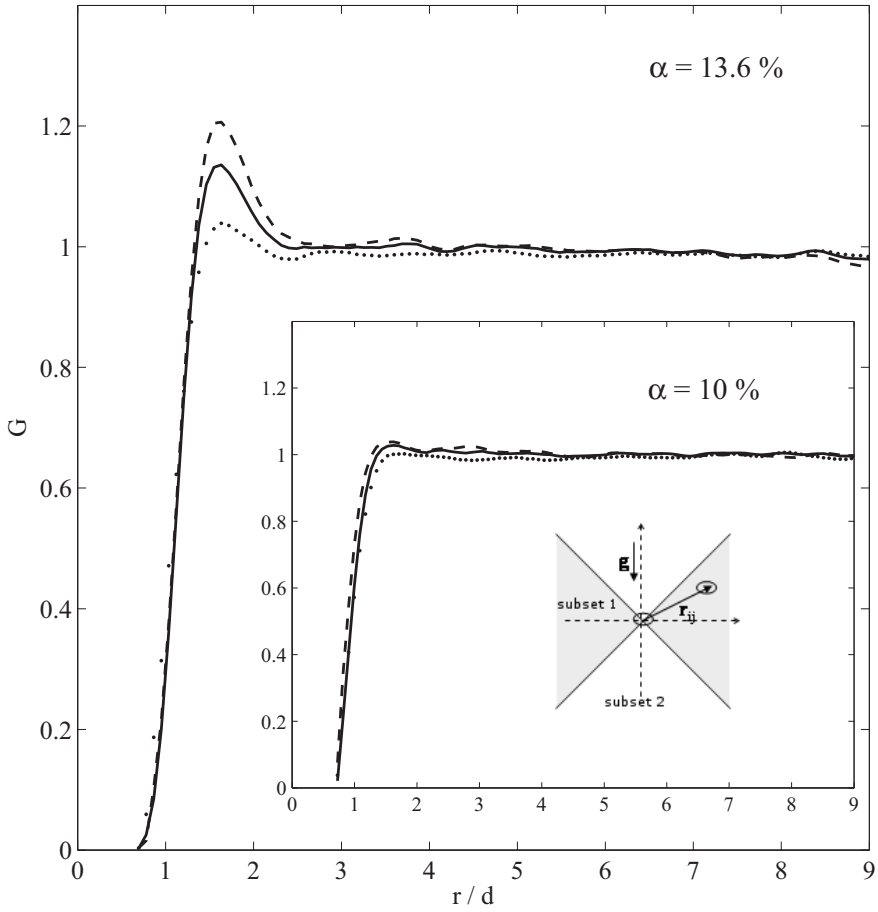

FIGURE 5. Radial pair distribution functions G for different alignments of bubble centers for α=13.6% or α = 10%. Dashed line, centers of each pair aligned about $\pm 45^\circ$ the horizontal direction (subset 1); dots, centers of each pair aligned about $\pm$ 45° the vertical direction (subset 2); plain line, all directions.

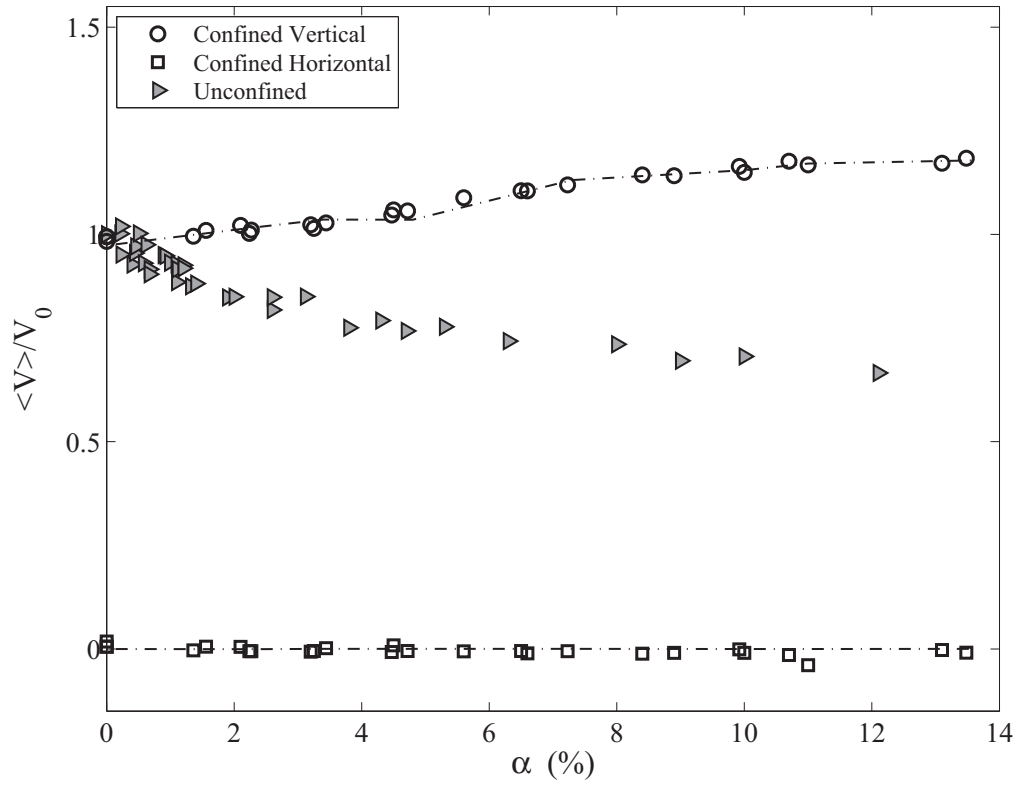

FIGURE 6. Mean bubble velocity normalized by the mean velocity of the single rising bubble. □, horizontal component $\langle V_y \rangle / V_0$; ∘, vertical component $\langle V_x \rangle / V_0$; △, vertical component in an unconfined bubble swarm from Riboux *et al.* (2010); $(-.-)$ $\langle V_{ux} \rangle$ and $\langle V_{uy} \rangle$ calculated by assuming that bubble locations are independent (Eq. 4.2).

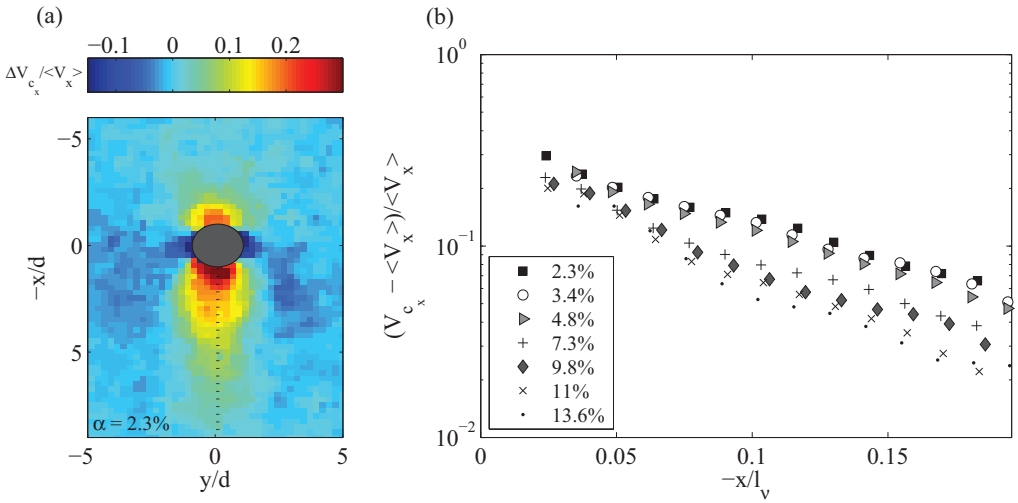

FIGURE 7. (a) Map of the difference between the vertical velocity of a bubble conditioned by the presence of a test bubble located at origin and the unconditional average velocity: $\Delta V_{c_x}(x,0)/\langle V_x\rangle$, for α =2.3%. (Positive values correspond to a velocity excess compared to the unconditional average velocity). (b) Vertical profile along the axis of symmetry behind the bubble. (It decays exponentially with a lengthscale proportional to the viscous scale $l_\nu = w^2 V_0/\nu$).

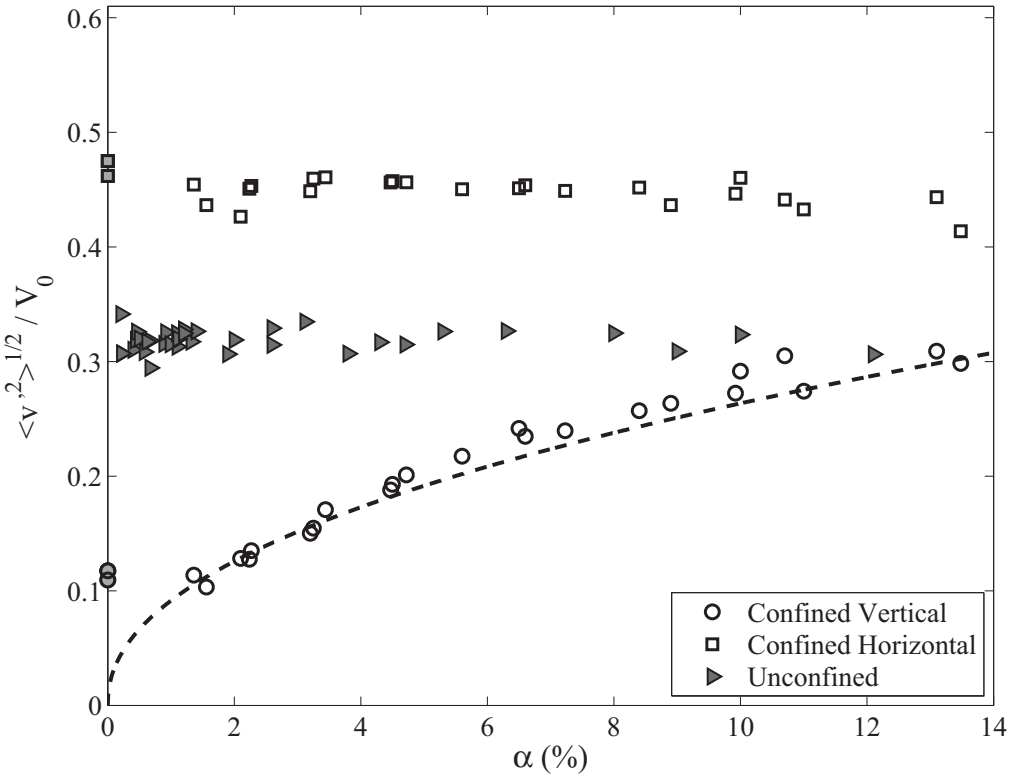

FIGURE 8. Standard deviation of the bubble velocity normalized by the mean velocity of single rising bubble. □, horizontal component $\langle v_y'^2 \rangle^{1/2}/V_0$; (○) vertical component $\langle v_x'^2 \rangle^{1/2}/V_0$ (in grey color at $\alpha = 0$ measurements for the isolated bubble). ▲, velocity characteristic of the global agitation in an unconfined bubbly flow from Riboux *et al.* (2010); For $\alpha \geqslant 1.4\%$, the normalized standard deviation in the vertical direction evolves as $0.76\alpha^{0.46}$ (Dashed line).

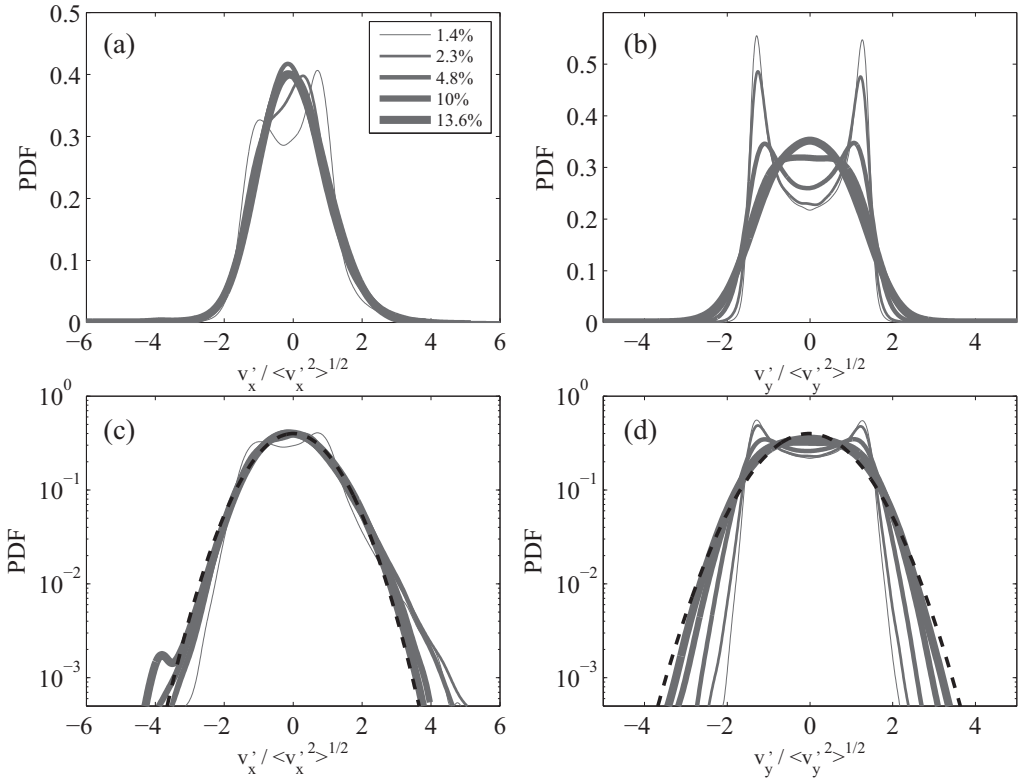

FIGURE 9. Normalized probability density functions of the velocity fluctuations for various gas volume fractions. (a) linear plot for vertical component; (b) linear plot for horizontal component; (c) semilog plot for vertical component; (d) semilog plot for horizontal component. Dashed lines in (c) and (d) represent Gaussian distributions.

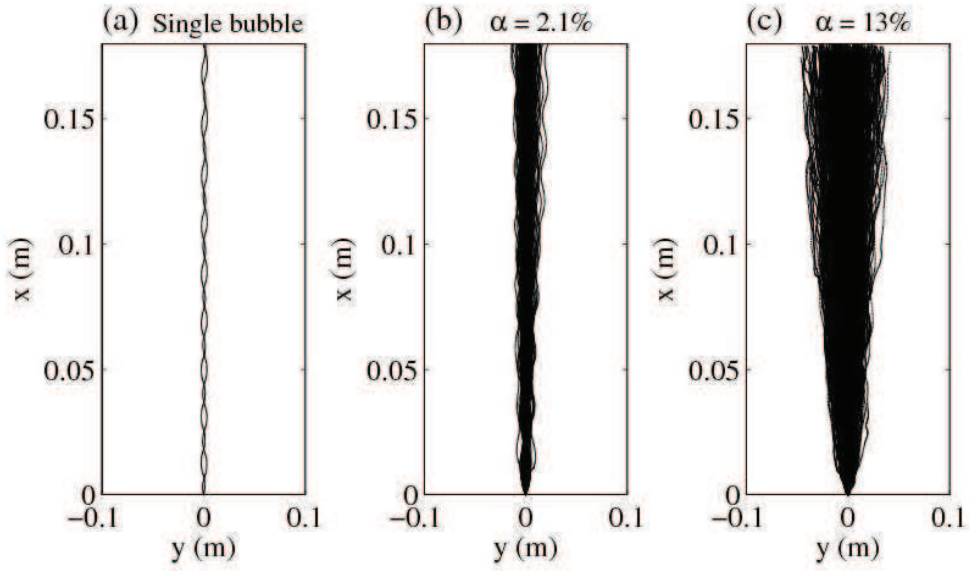

FIGURE 10. Superimposed bubble-center paths: (a), two isolated bubbles; (b), $\alpha = 2.1$ % (1,000 bubbles); (c), $\alpha = 13$ % (1,000 bubbles).

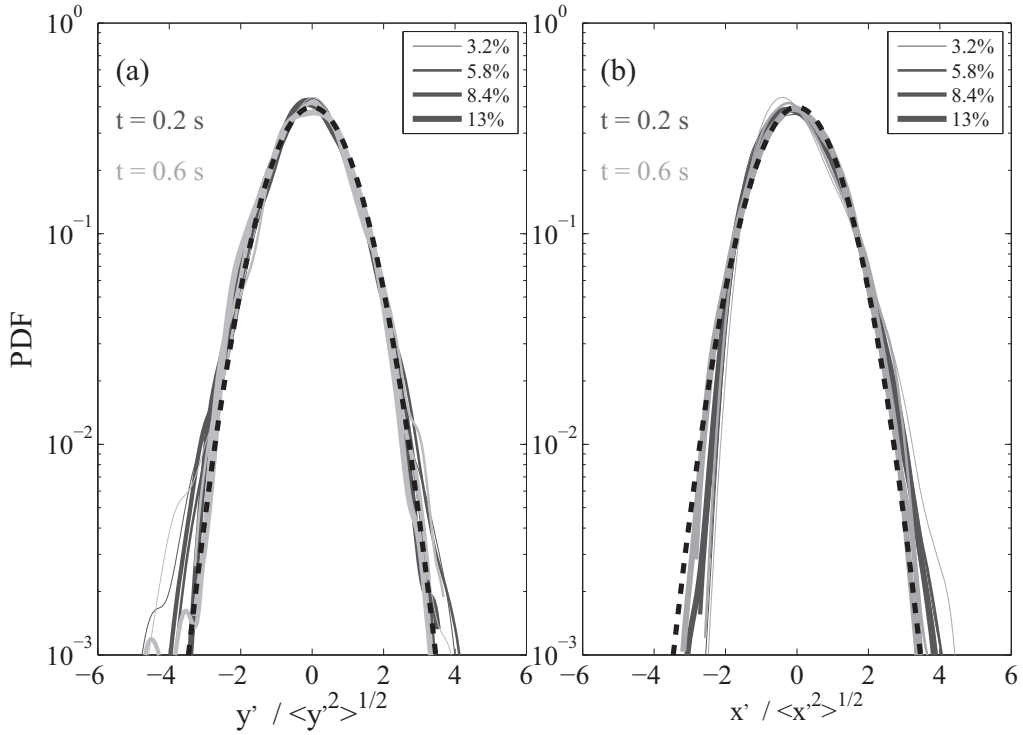

FIGURE 11. Normalized probability density functions of bubble-centre displacements at two different times after dispersion starts and for various gas volume fractions. (a), vertical direction; (b) horizontal direction. Dashed line represent Gaussian distribution.

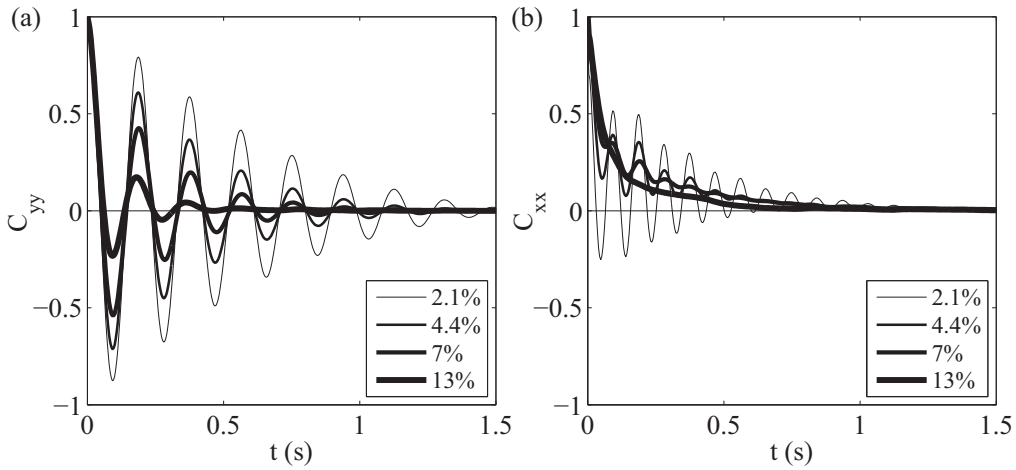

FIGURE 12. Lagrangian autocorrelation coefficients of the bubble velocity. (a), $C_{yy}(\tau) = \langle v'_y(t)v'_y(t+\tau)\rangle / \langle {v'_y}^2 \rangle$; (b), $C_{xx}(\tau) = \langle v'_x(t)v'_x(t+\tau)\rangle / \langle {v'_x}^2 \rangle$

.

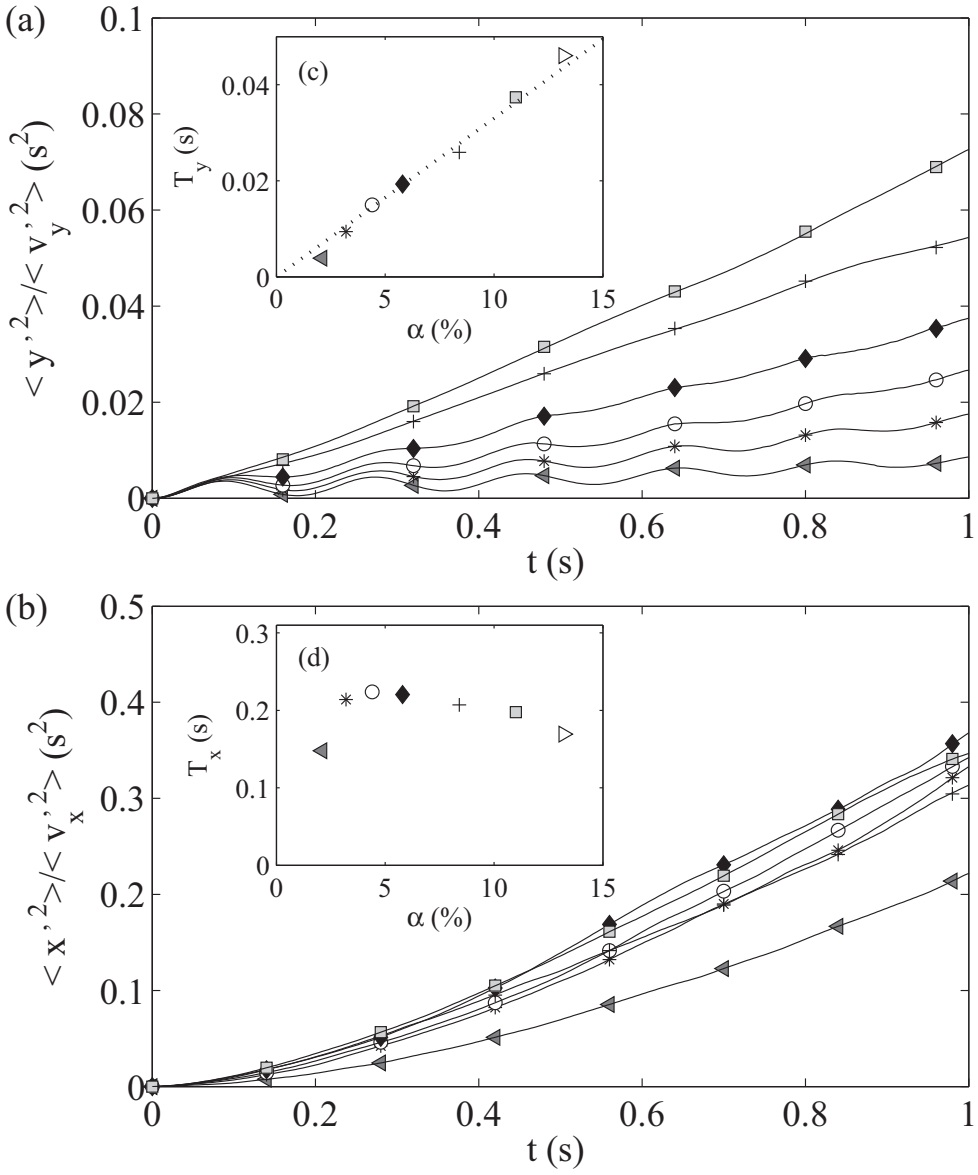

FIGURE 13. Variance of the bubble-centre displacements divided by bubble velocity variance for various gas volume fractions. (a), horizontal direction; (b), vertical direction. The insets show the corresponding Lagrangian integral timescale as a function of the gas volume fraction. The dotted line is a linear fit of the horizontal timescale: $T_y = 0.33\,\alpha$ s.

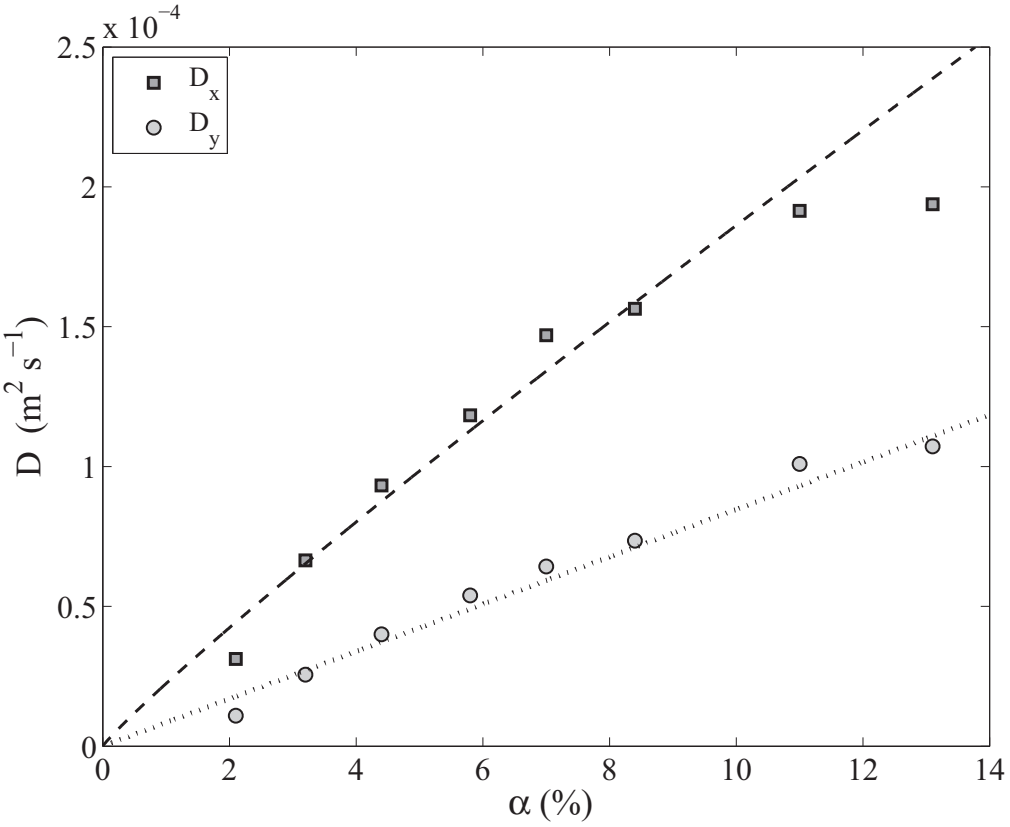

FIGURE 14. Evolution of the dispersion coefficients as a function of α. Dotted line: $D_x = \langle v_x'^2 \rangle \times T_x$ with $T_x = 0.21$ s and $\langle v_x'^2 \rangle = 7.4 \times 10^{-3}\,\alpha^{0.92}$ m^2·s^{-2}. Dashed line: $D_y = \langle v_y'^2 \rangle \times T_y$ with $T_y = 0.33\,\alpha$ s and $\langle v_y'^2 \rangle \approx 2.6 \times 10^{-3}$ m^2·s^{-2}